Dynamically-controlled variable-fidelity modelling for aircraft structural design optimisation

Jonathan G Allen, Graham Coates and Jon Trevelyan

School of Engineering and Computing Sciences, Durham University, United Kingdom

Abstract

Structural mass optimisation of an aircraft design is important in increasing the likelihood that a high quality airframe is designed of minimal weight whilst providing necessary resistance to load. Analysis of such structures is often performed at a single level of model fidelity, the selection of which can lead to either excessive computational time or reduced accuracy of results. Alternatively, variable-fidelity modelling may be employed to reduce such computational expense whilst maintaining accuracy, traditionally performed using predetermined levels of fidelity for specific periods of the optimisation process. This paper investigates dynamically-controlled variable-fidelity modelling (DCVFM) during aircraft conceptual design optimisation wherein fidelity is controlled as a dynamic parameter of the optimisation process. Consequently, model fidelity is adapted during optimisation to promote early discovery of promising design characteristics prior to detailed analysis of the best designs available. Models are constructed through the grouping of similar structural members within elements, thus reducing the

Corresponding author:

Jonathan Allen, School of Engineering and Computing Sciences, Durham University, South Road, Durham, DH1 3LE, United Kingdom.

Tel: +44 (0)1 191 334 2487

Email: j.g.allen@durham.ac.uk

number of degrees of freedom and subsequent computational effort required for analysis of each design. A case study is performed to verify the results of analysis and obtain benchmark results for optimisation with static model fidelity prior to the investigation of various set-ups of DCVFM. The results of this study indicate improved design quality using DCVFM compared to using static model fidelity whilst reducing the necessary computation time.

Keywords

Aircraft conceptual design, structural optimisation, variable-fidelity modelling, parameter control

Date received: *date*; revised: *date*; accepted: *date*

1. Introduction

The structural design of an aircraft concept is an important aspect of the overall design focussed on providing sufficient airframe mass and associated strength to withstand operational loads encountered in flight and on the ground. Excessive mass can diminish aircraft performance, e.g. fuel consumption, leading to increased costs and emissions [1,2]. This leads to the suitability of optimisation to achieve a design of minimal mass to ensure the aircraft meets vehicle performance requirements whilst also maintaining structural integrity under load [3-5].

Aircraft structural design optimisation is traditionally performed as an iterative process encompassing the set-up of the problem prior to modelling, analysis and optimisation of designs [3-7]. Problem set up includes the definition of the aircraft and mission requirements, selection of load cases, set-up of analysis tools, and input of optimisation parameters, i.e. operators and design variables, constraints and objectives [3]. The

profile of the aircraft is then generated, often including optimisation for minimal aerodynamic drag [4,6,8], for subsequent use as a boundary within which the structure is designed [3,5-7].

The airframe structure is modelled to enable analysis of its feasibility with respect to the design constraints, e.g. minimum factor of safety (FoS) under yield [2,5] or maximum wingtip deflection [7]. A finite element (FE) model is commonly subjected to analysis to approximate the response of the structure to the selected loads [4-6]. The accuracy of such finite element analysis (FEA) is dependent on the model fidelity, i.e. precision compared to reality, which also affects computational expense through determining the time required for modelling and analysis [9,10]. High-fidelity models provide greater precision than those of low fidelity, however the required modelling and analysis time can be prohibitively expensive due to the increase in the number of model degrees of freedom (DoF) [2,11]. This expense is increased further when evaluating multiple load cases or dynamic loads over many time steps [4]. However, precise analysis is desirable to ensure the optimisation process is correctly guided with regard to the feasibility of designs. Thus, a compromise is required between accuracy of results and computation time such that an adequate number of design variants may be considered during optimisation [7,11].

Variable-fidelity modelling uses multiple levels of model fidelity to reduce computational expense whilst maintaining reliability in results [8,12,13]. A typical approach employs a low-fidelity model at the start of the process to determine promising design characteristics at reduced computational expense before higher fidelity models are used for more detailed analysis of designs [11,14,15]. The static fidelity levels are conventionally input during problem set up, as are the points during the process at which fidelity changes [7,11-15]. This fails to offer the opportunity for dynamic adaptation of fidelity during optimisation for the improvement of design quality and computation speed.

A static process is traditionally employed for aircraft design optimisation [3]. However, earlier research has indicated a dynamic process can improve the quality of designs generated through adjustment of the optimisation technique employed and control of its parameters [16]. Parameter control modifies the values of process operators in order to encourage specific process behaviour, e.g. design quality, feasibility [16,17]. Different approaches to parameter control were investigated for the management of a genetic algorithm (GA), the results of which indicated significant improvements in design quality given appropriate bounds and rules [17]. Hence, parameter control may be suitable to enable dynamic adaptation of model fidelity during optimisation to encourage minimal runtime whilst maintaining design quality.

This paper introduces dynamically-controlled variable-fidelity modelling (DCVFM) for the adaptation of fidelity during structural optimisation such that discovery of high quality conceptual aircraft structural designs is encouraged at reduced computational expense. Optimisation is performed for the minimisation of airframe mass with design feasibility measured using FEA with respect to two design constraints:

c_1 minimum FoS under yield within the structure as defined by the von Mises criterion;

c_2 maximum wingtip deflection before ground strike.

An investigation into the effects of model fidelity and methods of parameter control on the designs generated is included. The remainder of the paper is organised as follows: the FE modelling process is described; DCVFM is presented; results obtained during FEA and optimisation are verified; a case study for structural optimisation of an existing aircraft design is performed; concluding remarks and suggestions for future work are given.

2. Modelling and analysis procedure

The feasibility of designs is determined during optimisation using FEA, the computational expense of which is defined by the time required to model the design and subsequently analyse its response, i.e. displacements and rotations due to load. Modelling time depends on the type of elements used and the size of the model, i.e. the number of nodes and elements to be constructed. Analysis time is dictated by the number of response evaluations and the size of the FEA problem. Loads are simulated as pseudo-static loads, as defined in [18], such that only a single evaluation is required per design load case. The size of the FEA problem is dependent on the type of elements and sizes of FEA matrices as defined by the number of DoF, i.e. the model size. One-dimensional beam elements model the structure to reduce computation whilst model size is defined by the structural design and level of model fidelity.

2.1 Construction of FE model

Model elements represent fuselage frames, floor beams and stringers as well as lifting surface ribs and spars. Skin is lumped within stringers due to the purpose of the latter to stiffen skin in resistance to buckling [19]. Lifting surface stringers are in turn lumped within spars as both provide resistance against bending [18]. The number of nodes, and therefore DoF, within the model is then reduced by grouping similar structural members into a smaller number of elements, thus reducing the model size. This paper differentiates between lumping and grouping by using the former to refer to combining different types of structural members of similar function, e.g. skin within stringers, whereas the latter refers to representing multiple members of the same type as a single element within the FE model to reduce the number of DoF, e.g. multiple ribs within a rib element. However, multiple spars are not grouped together in the FE model due to their importance in defining wingbox strength [18,19]. Grouping is performed using the following criteria:

(a) geometry;

(b) sectional properties;

(c) material properties.

Within the model, rectangular beam elements idealise the geometry of members of different cross-section, i.e. C, I, T and Z-sections. The centroid of the resulting element cross-section is positioned at the location corresponding to the central member grouped within the element. Element sectional properties are then determined using the parallel axis theorem before material properties are calculated as the surface area-weighted average of the properties of members, e.g. for the elastic modulus of the *e*th element, E^e

$$E^e = \sum_{i=1}^{n_m} \frac{A^i E^i}{A^e} \tag{1}$$

where A^e denotes the cross-sectional area of the *e*th element, whilst A^i and E^i signify the area and elastic modulus of the *i*th element member of the n_m members within the element. This grouping of members has the effect of smearing element properties, the extent of which increases with decreasing model fidelity. Smearing reduces the accuracy of results obtained through FEA; however the reduced model size lessens the subsequent computational effort required for FEA.

The extent of grouping is defined by model fidelity, F; the level of which denotes the approximate fraction of elements per member type. For example, a design with 100 frames modelled at F = 1.0 would model each frame explicitly whereas a model at F = 0.1 would model one in ten frames. In the latter, the frame elements would consist of the grouping of the nine frames closest to the elements. An example of the grouping of six members into two elements, i.e. F = 0.33, within a FE model is shown in Figure 1, where the central members, thus element centroid positions, are labelled as members 2 and 5.

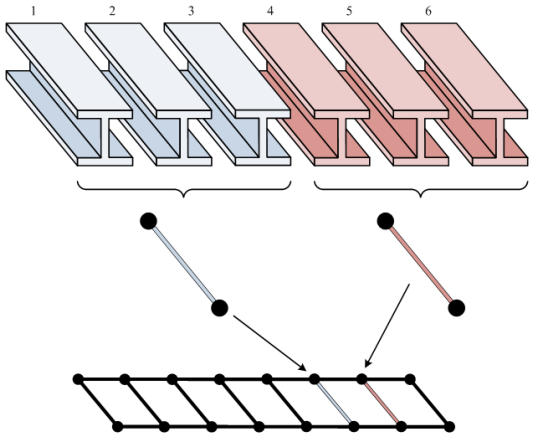

Figure 1. Example of member grouping.

2.2 Recovery of member stress field

The response of the model to pseudo-static load is calculated by Gaussian elimination with back-substitution of the static equation of motion (EoM)

$$\boldsymbol{f} = \mathbf{K}\boldsymbol{u} \tag{2}$$

where $\boldsymbol{f}$ represents the applied load, $\mathbf{K}$ the model stiffness and $\boldsymbol{u}$ the response of the model, i.e. displacements and rotations. Subsequently, the internal force within an element as a result of its response is determined by solving the EoM for the element. Furthermore, the force within each of the n_m element members is found for DoF j as

$$f_j^i = \frac{f_j^e}{\sum_{k=1}^{n_m} \gamma_j^i / \gamma_j^k} \tag{3}$$

where f_j^e and f_j^i denote the internal forces within the *e*th element and *i*th element member respectively in the *j*th DoF. Symbols f_1^i, f_2^i and f_3^i represent the internal forces within the *i*th member in the *x*, *y* and *z* directions respectively. Similarly, f_4^i, f_5^i and f_6^i signify the moments of the *i*th member about the *x*, *y* and *z* axes respectively. Factors γ_j^i and γ_j^k are defined by DoF *j* and the properties of the *i*th and *k*th members. Therefore the distribution of element force to the *i*th, or similarly *k*th, element member is defined by the following factors

$$\gamma_1^i = \frac{l^i}{E^i A^i} \tag{4a}$$

$$\gamma_2^i = \frac{l^i}{E^i I_{zz}^i} \tag{4b}$$

$$\gamma_3^i = \frac{l^i}{E^i I_{yy}^i} \tag{4c}$$

$$\gamma_4^i = \frac{l^i}{G^i I_p^i} \tag{4d}$$

$$\gamma_5^i = \gamma_6^i = \frac{l^i}{G^i A^i} \tag{4e}$$

where l^i defines the length; I_p^i, I_{yy}^i and I_{zz}^i the second moments of area about the polar *x* and cross-sectional *y* and *z* axes; and G^i the shear modulus of the *i*th element member. The expressions of equation (4) are developed by assuming equilibrium among element members in the corresponding DoF. These assumptions

are made using the classical approach to a statically indeterminate problem. For example, it is assumed that there is equal axial extension of the element and its members. Consequently, the eth element axial force, f_1^e, may be expressed as the sum of the corresponding forces in the n_m element members by assuming equal extension, u_x^e, of the element and its members. The resulting expression given the static EoM in equation (2) and Hooke's law is

$$f_1^e = \sum_{i=1}^{n_m} \frac{E^i A^i}{l^i} u_x^e \tag{5}$$

Equation (3) is therefore obtained for f_1^i by substituting equation (4a) into equation (5) and rearranging the resulting expression for the axial force in the *i*th element member. Equation (3) is similarly obtained for the remaining DoF by correspondingly assuming equilibrium of the element and its members in shear angle (f_2^i and f_3^i using equations (4b) and (4c) respectively), twist (f_4^i using equation (4d)) and slope (f_5^i and f_6^i using equation (4e)). The stress field at both ends of each member is then evaluated using established formulae [20] at a series of points on the member cross-section. The points selected are those expected to generate a maximum stress in any DoF *j*, for example such points on an I-section are illustrated in Figure 2.

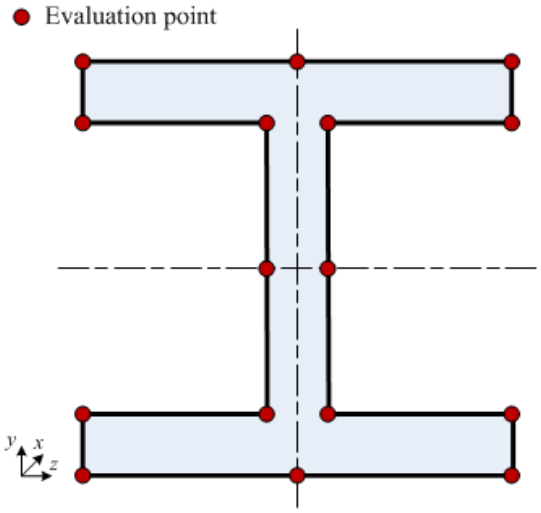

Figure 2. I-section stress evaluation points.

The principal stresses and corresponding FoS as defined by the von Mises criterion are calculated at each point. Similarly, the FoS with respect to the Euler buckling load and maximum bending stress of simply-supported beams are also determined [18,19]. Consequently, the feasibility of a design is determined by comparing the lowest FoS within the structure against c_1 and the wingtip nodal deflection against c_2.

3. Parameter control within DCVFM

DCVFM is performed through the inclusion of model fidelity as a variable of parameter control. The method of parameter control, which is chosen during problem set-up, can be deterministic, hyper-heuristic or self-adaptive.

3.1 Deterministic control

The following time-based rule is applied such that model fidelity increases during optimisation

$$F\left(t\right) = F_{\min} + \frac{\left[\beta\left(t\right)\left(F_{\max} - F_{\min}\right)\right]^{\delta}}{\left(F_{\max} - F_{\min}\right)^{\delta-1}} \tag{6}$$

where $F(t)$ defines model fidelity at generation t as constrained between $F_{\min} \leq F(t) \leq F_{\max}$, and $\beta(t)$ denotes a weighting factor associated with the generation number of the optimisation process

$$\beta\left(t\right) = \frac{t}{t_{\max}} \tag{7}$$

where t and $t_{\max}$ indicate the current and final generation number of the process respectively. It should be noted that herein a population-based optimisation technique is used. Parameter δ controls the rate of change of model fidelity, where $\delta > 0$. The rule defined by equation (6) encourages low-fidelity analysis at the start of the process prior to more detailed analysis at higher fidelity during later generations. This reduces the computational expense required to establish good characteristics of designs before performing more precise analysis of good designs for a more accurate determination of feasibility. Existing approaches to variable-fidelity modelling typically incorporate discrete changes in fidelity at specific points during the process, whereas herein modification is continuous.

3.2 Hyper-heuristic control

Hyper-heuristics modify the set-up of the optimisation process to encourage improved performance through the maximisation of a hyper-heuristic objective function formed using components of process performance, e.g. higher quality of designs or reduced computational time [21]. A heuristic or meta-heuristic modifies the set-up of the process by varying the optimisation techniques and process parameters [22]. A previous study

indicated hyper-heuristic parameter control performed well when coupled with deterministic control [17]. As a result, hyper-heuristic control is performed by varying δ within the deterministic rule, equation (6), to adapt the rate at which model fidelity changes, i.e. δ becomes $\delta(t)$. This is performed by a simulated annealing (SA) hyper-heuristic to perturb the value of $\delta(t)$ at each generation. Each new value of $\delta(t)$ is accepted if permitted by the SA cooling schedule [23] or an improvement is made in the hyper-heuristic objective function

$$\phi\left(t\right) = \beta\left(t\right)\phi_1\left(t\right) + \left(1 - \beta\left(t\right)\right)\phi_2\left(t\right) \tag{8}$$

where $\phi(t)$ is the hyper-heuristic objective value at generation t to be maximised through components

$$\phi_1\left(t\right) = \frac{\min\left(\Phi\left(t\right), \Phi\left(t-1\right)\right)/2}{\Phi\left(t\right)} \tag{9a}$$

$$\phi_2\left(t\right) = \frac{\min\left(T\left(t\right), T\left(t-1\right)\right)/2}{T\left(t\right)} \tag{9b}$$

where $\Phi(t)$ and $T(t)$ denote the problem objective value, i.e. structural mass, and the computation time taken for generation t. The value of $\phi(t)$ is compared with $\phi(t-1)$, computed by equation (8) for the previous generation using the components

$$\phi_1\left(t-1\right) = \frac{\min\left(\Phi\left(t\right), \Phi\left(t-1\right)\right)/2}{\Phi\left(t-1\right)} \tag{10a}$$

$$\phi_2\left(t-1\right)=\frac{\min\left(T\left(t\right),T\left(t-1\right)\right)/2}{T\left(t-1\right)} \tag{10b}$$

The numerators of equations (9) and (10) limit the components to $0 \leq \phi_{1,2}(t) \leq 0.5$ for generation t such that $0 \leq \phi(t) \leq 1$ and similarly for $t - 1$. An improvement is recorded if $\phi(t) > \phi(t - 1)$. This function is similar to that of [21] but differs in its application and through the components used.

3.3 Self-adaptive control

Self-adaptive control encodes parameters within the designs undergoing optimisation as additional design variables [24]. Therefore, each individual design possesses its own values of controlled parameters independent from all other designs. For example, a design initially possessing n design variables would encode the first self-adaptive parameter as v_{n+1}. As a result, the model fidelity level is appended to the design variables of each individual such that $F = v_{n+1}$, leading to the coevolution of the design and parameter by the applied optimisation technique. Such quality-based control differs from the methods of deterministic, i.e. time-based, and hyper-heuristic, i.e. quality and time-based, control.

4. Case study

An investigation is performed into the effects of DCVFM on the airframe designs generated during optimisation, and the corresponding computational expense, compared to those obtained with static model fidelity. This investigation is performed in three stages:

1. Design feasibility is measured using FEA at different levels of model fidelity to establish the corresponding variation in the precision of FEA results and required computation time.

2. Optimisation is performed using static levels of fidelity to determine the best designs generated and computational expense of such simulations.
3. Optimisation is similarly performed using DCVFM to examine its effects on the designs obtained and computational expense.

The Embraer 195 (E-195), a large civil aircraft, is the subject of the study. Table 1 lists a selection of the properties of the aircraft [25,26] and its mission. The powerplant of the E-195 is currently subject to re-engineering for improved fuel performance, although Embraer previously considered a redesign of the existing E-195 airframe [27]. Consequently this aircraft is selected to demonstrate the potential reduction in structural mass that can be achieved, which can lead to improved fuel performance [2]. The selected load case to be applied is the maximum load within the flight envelope, a +2.5 g symmetric pull-up manoeuvre [28], in combination with cabin pressurisation, engine thrust, and gravity.

Table 1. Properties of Embraer 195 aircraft.

Property	Value
Wing span	28.72 m
sweep	27.0 º
Tail span	12.09 m
height	10.57 m
Fuselage length	38.67 m
height	3.35 m
Undercarriage track	5.94 m
wheelbase	14.64 m
Powerplant	2x GE CF34-10E
Mass operating empty	28,970 kg
maximum takeoff	48,790 kg
Cruise altitude	35,000 ft
range	1,400 nm
speed	0.8 M
Number of flight crew	2
passengers	118

4.1 Effects on design feasibility of model fidelity

Model fidelity affects FEA precision, inaccuracies in the results of which can misguide optimisation in terms of design feasibility. Results of FEA are verified at 10 equally-spaced levels of static model fidelity for 20

arbitrary structural designs within the profile of the E-195. Only the starboard side of the aircraft is analysed as the load case is symmetric along the longitudinal axis of the vehicle. The fidelity levels investigated are listed in Table 2. A minimum value of $F = 0.1$ is set to ensure a sufficient quantity of nodes for modelling the aircraft. The results of the investigation are also presented in Table 2. These include the mean number of DoF, n_{DoF}, for the modelled designs alongside $\Delta c_{1,2}$ to denote the mean difference in the values measured with respect to the design constraints for minimum FoS under the von Mises criterion, c_1, and wingtip deflection, c_2, compared to those corresponding to the model at $F = 1.0$, i.e. at highest fidelity and greatest expected accuracy.

Table 2. Variations in n_{DoF} and $\Delta c_{1,2}$ with F.

F	n_{DoF}	Δc_1	Δc_2 (m)
0.1	1,566	0.9712	0.0108
0.2	2,420	0.7419	0.0107
0.3	3,718	0.2593	0.0051
0.4	5,193	0.0000	0.0061
0.5	7,113	0.0000	0.0090
0.6	8,983	0.0000	0.0091
0.7	10,563	0.0000	0.0084
0.8	11,125	0.0000	0.0049
0.9	12,767	0.0000	0.0017
1.0	15,671	-	-

Table 2 indicates small differences in the values of $c_{1,2}$ compared to n_{DoF}. At $F \geq 0.4$, negligible difference was observed in Δc_1, whilst at $F < 0.4$ Δc_1 increased with decreasing F, as to be expected with reduced model precision. This is a valuable observation given that earlier experimentation has determined c_1 as the critical design constraint [16]. Limited variation in Δc_2 was observed throughout. These results indicate negligible difference in the feasibility measured at $F \geq 0.4$, thus providing confidence that such variation in model fidelity will not adversely affect the optimisation process.

Figure 3 plots the variation in n_{DoF} and the mean computation time for modelling and analysis, T, against fidelity, F. The time taken at $F = 0.1$ was 0.04% of that required at $F = 1.0$. Such a reduction in computational expense is beneficial during lengthy optimisation problems, especially given the small differences measured in feasibility at various fidelities. A reduction in T occurs between $F = 0.7$ and $F = 0.8$ even though n_{DoF} increases, most likely due to increased banding of the FEA matrices as a result of the different FE models. Figure 4 illustrates the FE models at a sample of fidelity levels. As fidelity rises, there is a clear increase in the number of elements and nodes, thus DoF; leading to reduced smearing and superior precision but increased computational expense. Given the findings of this investigation, the remaining stages of this study are conducted at $F \leq 0.4$ to reduce the required runtime of the study.

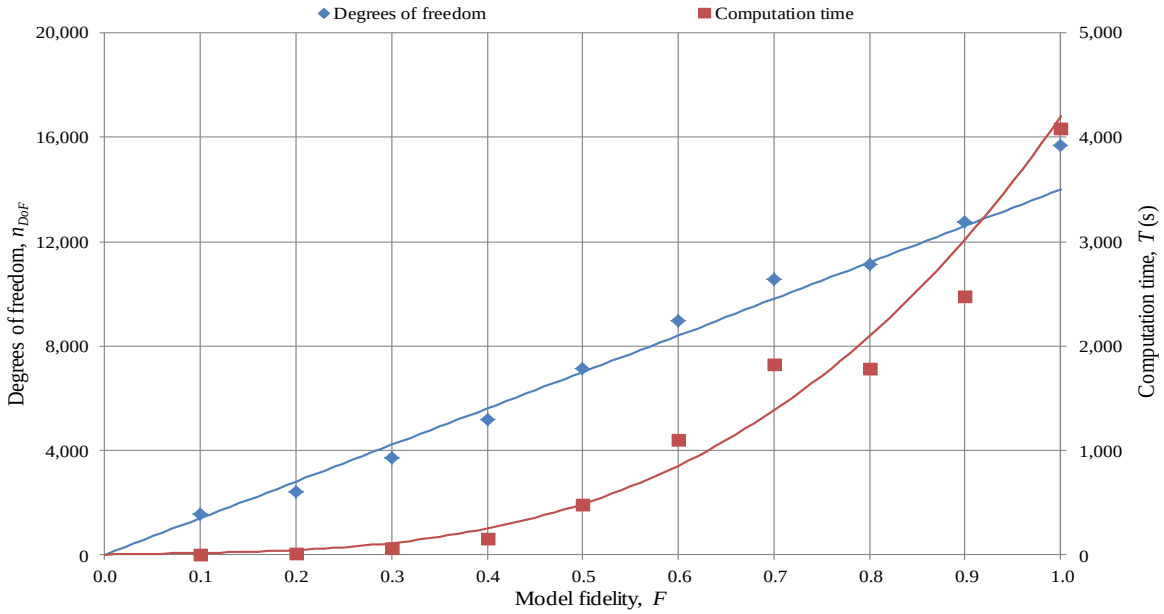

Figure 3. Variations in n_{DoF} and T with increasing levels of model fidelity, F.

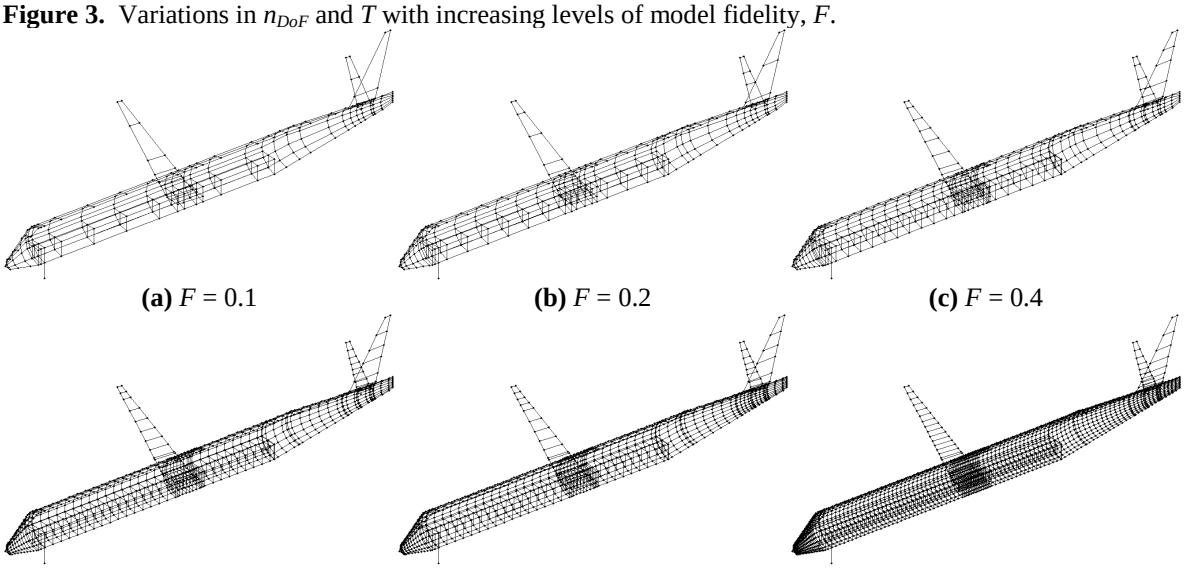

(a) F = 0.1 **(b)** F = 0.2 **(c)** F = 0.4

(d) F = 0.6 **(e)** F = 0.8 **(f)** F = 1.0

Figure 4. FE models of E-195 structural designs at a sample of model fidelity levels.

4.2 Optimisation with static model fidelity

Optimisation is performed using static levels of model fidelity to provide benchmarks of results for future comparison against those obtained using DCVFM. Furthermore, verification is made that the small losses in FEA precision recorded in the previous investigation do not misguide the optimisation process. Such misguidance is possible as high quality designs of low mass may be expected to be marginally feasible, i.e. close to the constraint boundaries [29]; thus small losses in precision can lead to feasible designs being deemed infeasible at low fidelity, or vice versa.

The optimisation problem is independently solved at four levels of fidelity: F = 0.1, 0.2, 0.3 and 0.4, with five experiments performed at each level to account for variability due to the stochastic GA-based optimisation. A population of 100 designs is optimised over 1,000 generations using a GA with roulette wheel selection, one-point crossover at 90% probability, and Gaussian mutation at 1% probability. An exterior penalty function penalises the quality, i.e. structural mass, of infeasible designs that violate the design constraints. The materials, profiles, and geometries of the structural members are presented in Table 3.

Table 3. Material, profile and geometry of structural members types.

Member type	Material	Profile	Thickness (mm)	Height (mm)	Width (mm)
Frames	Al 7075-T6	T	5	80	80
Floor beam	Al 7075-T6	I	Web: 15; Flange: 20	Total: 100; Web: 80	50
Ribs	Al 7075-T6	I	Web: 5; Flange: 5	Location-dependent	8
Spars	Al 7178-T6	I	Web: 4; Flange: 30	Location-dependent	60
Stringers	Al 2014-T6	Z	2	20	20
Skin	Al 2014-T6	-	2	-	-
Floor	Al 7075-T6	-	20	-	-

The aircraft structural layout is defined by the design variables in Table 4. Variables v_1 to v_8 define the quantity of structural members, whilst lifting surfaces are constrained to possess two spars each. Variables v_3 and v_7 indicate the number of ribs in each horizontal lifting surface whilst v_4, v_6 and v_8 indicate the number of stringers on each face of each lifting surface. Variables v_9 to v_{11} define the spanwise distribution the rth rib as

$$y_r = \frac{r^{\alpha-1}\left(Cb - y_0\right)}{n_r^{\alpha}} + y_0 \tag{11}$$

where α represents v_9, v_{10} or v_{11} and n_r correspondingly represents v_3, v_5 or v_7 for the horizontal tail, vertical tail and wing respectively, e.g. $\alpha = v_9$ and $n_r = v_3$ for the horizontal tail. The lifting surface span is defined by b and root rib position by y_0. The constant C equals 0.5 for horizontal and 1.0 for vertical surfaces. The chordwise position of the front wing spar is defined by v_{12} as a fraction of wing chord, c_w, with the remaining spars positioned empirically [30]. Variables v_{13} to v_{15} define the distribution of frames to the nose, wingbox

and tail, whilst floor beams are positioned at cabin frame locations. Design constraints are determined by the airworthiness requirements [28] and the maximum wingtip deflection before ground strike [25].

The best designs generated at each level of fidelity are included in Table 4. Variations were observed in the designs generated using different levels of fidelity, most noticeably in the number and distribution of fuselage members as expected due to stochastic optimisation and varied member grouping at different fidelity levels. Nevertheless, similar values for most variables were found leading to comparable design mass and feasibility. This indicates that the optimisation process is not prohibitively affected by decreasing model fidelity, even if different final designs are generated. These results also indicate decreasing final design mass with increasing fidelity.

The best design found with $F = 0.4$ was infeasible due to a frame possessing a FoS marginally below the design constraint, indicating the frame design was located in close proximity to the constraint boundary. The best design at $F = 0.1$ was 12.4% heavier than that at $F = 0.4$, principally due to the increase in frames and thus floor beams. However, runtime at $F = 0.4$ was 4.1 times of that at $F = 0.1$. High performance computing resources were employed for parallel analysis of each generation of designs during all experiments. This was essential to reduce runtime below a hardware constraint, for example the mean time required at the highest level of fidelity considered, $F = 0.4$, would have been 13.2 days without the use of parallel programming. Parallel analysis was performed over 20 computing nodes, each comprising of two 6-core Intel E5645/2.4 GHz Nehalem Westmere processors with 4 GB of memory per core and QDR integrated InfiniBand interconnect. Therefore, each population generation of 100 individuals was analysed in five groups of 20 designs with each design analysed on a separate node. The designs in Table 4 are illustrated in Figure 5, indicating a noticeable reduction in the number of fuselage members with increasing model fidelity. It should

be noted that this representation of the aircraft shows the airframe itself, i.e. not the FE model at a specific level of fidelity.

Table 4. Ranges of design variables and best designs generated using different levels of model fidelity.

		Range		Level of model fidelity, F			
Symbol	Design parameter	Min.	Max.	0.1	0.2	0.3	0.4
v_1	Number of fuselage frames	8	100	51	33	33	34
v_2	fuselage stringers	8	120	22	70	49	36
v_3	horizontal tail ribs	2	50	3	3	3	9
v_4	horizontal tail stringers	2	100	30	32	32	30
v_5	vertical tail ribs	2	50	3	3	3	3
v_6	vertical tail stringers	2	100	34	35	35	35
v_7	wing ribs	2	100	6	7	7	7
v_8	wing stringers	2	120	20	21	21	20
v_9	Position of horizontal tail ribs	1.00	3.00	1.59	1.00	1.00	1.00
v_{10}	vertical tail ribs	1.00	3.00	1.00	1.00	1.14	1.00
v_{11}	wing ribs	1.00	3.00	1.79	1.33	1.00	1.62
v_{12}	wing front spar root (c_w)	0.20	0.35	0.35	0.25	0.30	0.31
v_{13}	Distribution of frames to nose (%)	5.00	15.00	10.69	15.00	13.15	12.09
v_{14}	frames to wingbox (%)	5.00	15.00	15.00	5.00	6.80	5.60
v_{15}	frames to tail (%)	5.00	15.00	10.55	11.21	13.75	9.72
Φ	Structural mass (kg)			10,864	9,787	9,673	9,666
c_1	Minimum von Mises FoS	1.50		1.50	1.50	1.50	1.49
c_2	Wingtip deflection (m)	-3.40	3.40	-0.06	0.12	0.19	0.11
T	Computation time (h)			3.49	6.11	8.73	14.44

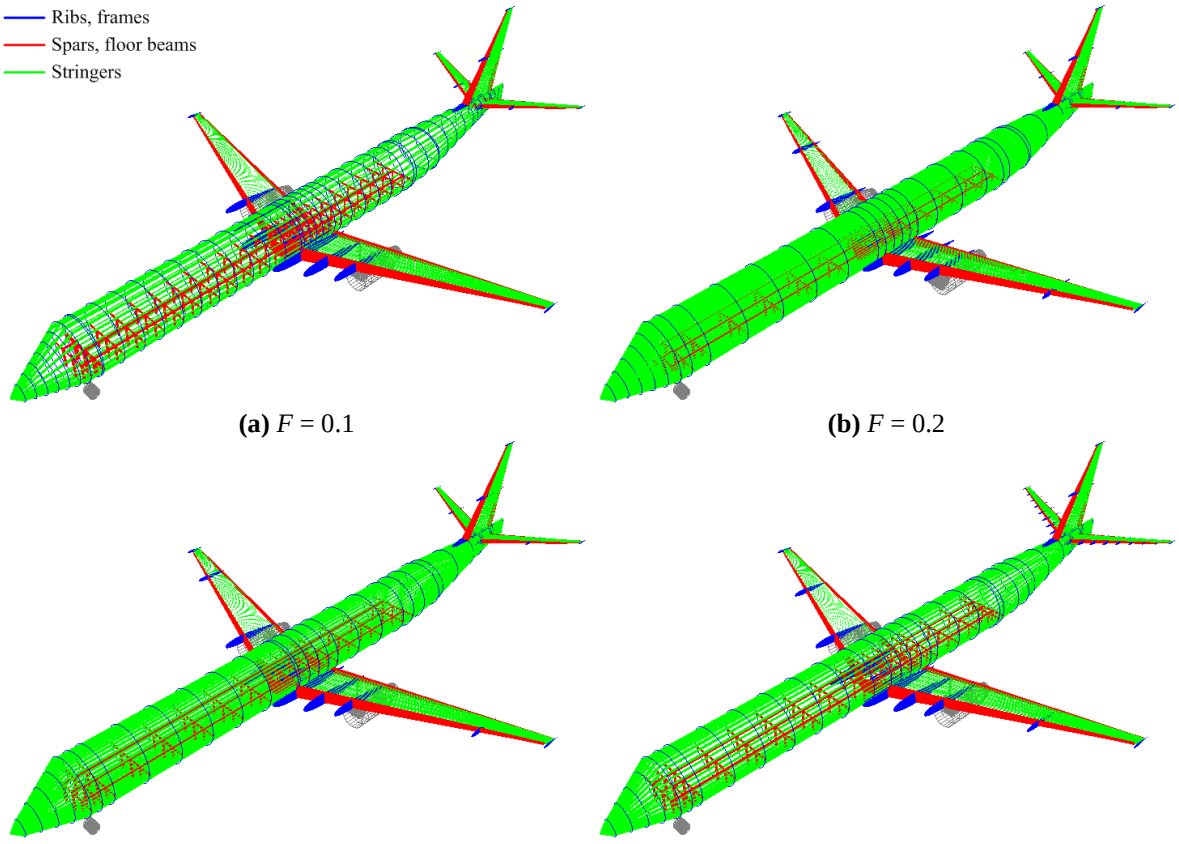

(a) F = 0.1 **(b)** F = 0.2

(c) F = 0.3 **(d)** F = 0.4

Figure 5. Models of best aircraft designs generated using different levels of model fidelity during FEA.

4.3 Optimisation incorporating DCVFM

Optimisation is conducted using DCVFM for a comparison of results against those obtained using different levels of static model fidelity. Table 5 lists the 13 different set-ups of DCVFM investigated. Cases 1 to 7 investigate deterministic control of model fidelity using various rates of increase in fidelity, i.e. δ in equation (6). The minimum and maximum values of δ are selected as the reciprocals of each other, i.e. ¼ and 4, to suitably bound the investigation. Cases 8 to 11 investigate hyper-heuristic control with various limits on $\delta(t)$,

the values of which are selected to evaluate the effects of constraints on the performance of DCVFM. Case 12 applies self-adaptive control of F by encoding fidelity as an additional design variable, v_{16}. Case 13 performs variable-fidelity modelling representative of that employed in [14] to allow a comparison to be made between DCVFM and a traditional approach. Model fidelity is increased from $F = 0.1$ to $F = 0.4$ through discrete steps of $\Delta F = 0.06$ every 180 generations, resulting in five equal increases of fidelity during the optimisation process.

The optimisation process is set up as described in the previous section so that results may be compared against the benchmarks obtained with static levels of fidelity; hence DCVFM is bounded to $0.1 \leq F \leq 0.4$. Five experiments are performed for each case to address variability in results due to stochastic optimisation whilst limiting the required runtime of the study to an acceptable value.

Table 5. DCVFM set-up for case study.

Case	Parameter control	DCVFM set-up
1	Deterministic	$\delta = 0.25$
2	Deterministic	$\delta = 0.5$
3	Deterministic	$\delta = 0.75$
4	Deterministic	$\delta = 1$
5	Deterministic	$\delta = 2$
6	Deterministic	$\delta = 3$
7	Deterministic	$\delta = 4$
8	Hyper-heuristic	$0.1 \leq \delta(t) \leq 1.0$
9	Hyper-heuristic	$0.1 \leq \delta(t) \leq 2.0$
10	Hyper-heuristic	$1.0 \leq \delta(t) \leq 3.0$
11	Hyper-heuristic	$1.0 \leq \delta(t) \leq 5.0$
12	Self-adaptive	$F = v_{16}$
13	Discrete	$\Delta F = 0.06$

Table 6 presents the best designs generated across all experiments performed for each case in Table 5.

Table 6. Values of design parameters for best designs generated during each case.

Design	Case												
parameter	1	2	3	4	5	6	7	8	9	10	11	12	13
v_1	32	32	33	33	35	33	34	32	34	33	32	35	49
v_2	46	46	46	46	40	46	42	46	49	49	46	43	27
v_3	3	3	3	3	3	3	3	3	3	3	3	3	3
v_4	32	32	28	32	29	26	38	34	27	35	27	32	36
v_5	3	3	3	3	3	3	3	3	3	3	3	3	3
v_6	35	35	32	36	39	32	42	35	34	35	33	35	37
v_7	7	7	8	7	7	7	7	7	8	7	7	7	7
v_8	21	20	19	20	23	18	25	22	19	21	20	21	23
v_9	1.00	1.00	1.00	1.00	1.00	1.00	1.00	1.00	1.11	1.00	1.00	1.00	1.00
v_{10}	1.00	1.00	1.00	1.00	1.00	1.00	1.00	1.00	1.00	1.00	1.00	1.00	1.00
v_{11}	1.00	1.00	1.00	1.00	1.00	1.00	1.00	1.00	1.00	1.00	1.38	1.17	1.00
v_{12} (c)	0.32	0.31	0.33	0.25	0.31	0.25	0.21	0.33	0.23	0.25	0.31	0.27	0.35
v_{13} (%)	13.19	14.51	14.34	14.34	10.54	15.00	15.00	13.52	14.19	15.00	13.36	15.00	12.73
v_{14} (%)	5.00	5.00	5.00	5.72	6.85	8.86	8.76	5.00	6.00	5.00	5.00	6.17	9.86
v_{15} (%)	13.03	14.06	9.03	13.29	15.00	9.58	8.21	14.11	15.00	12.77	13.45	13.34	12.84
Φ (kg)	9,535	9,536	9,671	9,583	9,756	9,613	9,818	9,543	9,665	9,612	9,562	9,669	9,956
c_1	1.50	1.50	1.50	1.50	1.50	1.50	1.51	1.49	1.49	1.47	1.49	1.50	1.50
c_2 (m)	0.20	0.20	0.11	0.16	0.19	0.18	0.14	0.20	0.08	0.16	0.15	0.14	0.23
T (h)	8.31	7.38	8.19	10.92	13.04	8.28	10.46	9.56	13.32	10.69	8.73	13.08	8.80

The results of Table 6 indicate improvement in the designs generated using DCVFM for Cases 1, 2, 4, 6, 8, 9, 10 and 11 compared to those obtained with static model fidelity, i.e. those in Table 4. Furthermore, decreased computation time was witnessed for these cases without a loss in design quality. Early discovery of promising design characteristics at low-fidelity were observed for Cases 1, 2 and 8 prior to further improvements at higher fidelity. In these cases, small values of δ or $\delta(t)$ led to the final design in fewer generations than in other cases. For example, the best design for Case 1, also the best design overall, was obtained in generation 341 after 3.1 h compared to generation 974 after 14.2 h for the best design with static fidelity, i.e. $F = 0.4$. Further, the quickest discovery of a best design with static fidelity was found after 3.4 h at generation 977 with $F = 0.1$. More specifically, the best design in Case 1 was 1.4% lighter than the best with $F = 0.4$ and was found in 21.6% of the time. Cases 3, 5, 7 and 12 generated worse designs than for $F = 0.4$, although only marginally for Cases 3 and 12. The loss of quality was caused by too many generations performed at low-fidelity due to the higher values of δ or $\delta(t)$ lower bound. However, Case 13 generated a considerably heavier design using discrete variable-fidelity modelling than for all other cases and static levels of fidelity except at $F = 0.1$.

The variation in model fidelity over optimisation generations is illustrated for each case in Figure 6. The effects of varying δ are identifiable for Cases 1 to 7. Similarly, the general increase in fidelity with hyper-heuristic control is evident for Cases 8 to 11 due to the underlying use of equation (6), with additional perturbation of $\delta(t)$ evident by the non-uniform variation of F. The fidelity of the running optimum during self-adaptive control of Case 12, i.e. v_{16}, is similarly shown, indicating early selection of a high-fidelity model. The discrete changes to fidelity made during Case 13 every 180 generations are also shown. The early increases in F during Cases 1, 2 and 8 that led to quicker discovery of the best designs are also visible in Figure 6. This confirmed that model fidelity should begin at a low value for a short period of generations

prior to a steep increase in order to minimise the computational time required to generate a high quality design, i.e. $\delta \leq 1$.

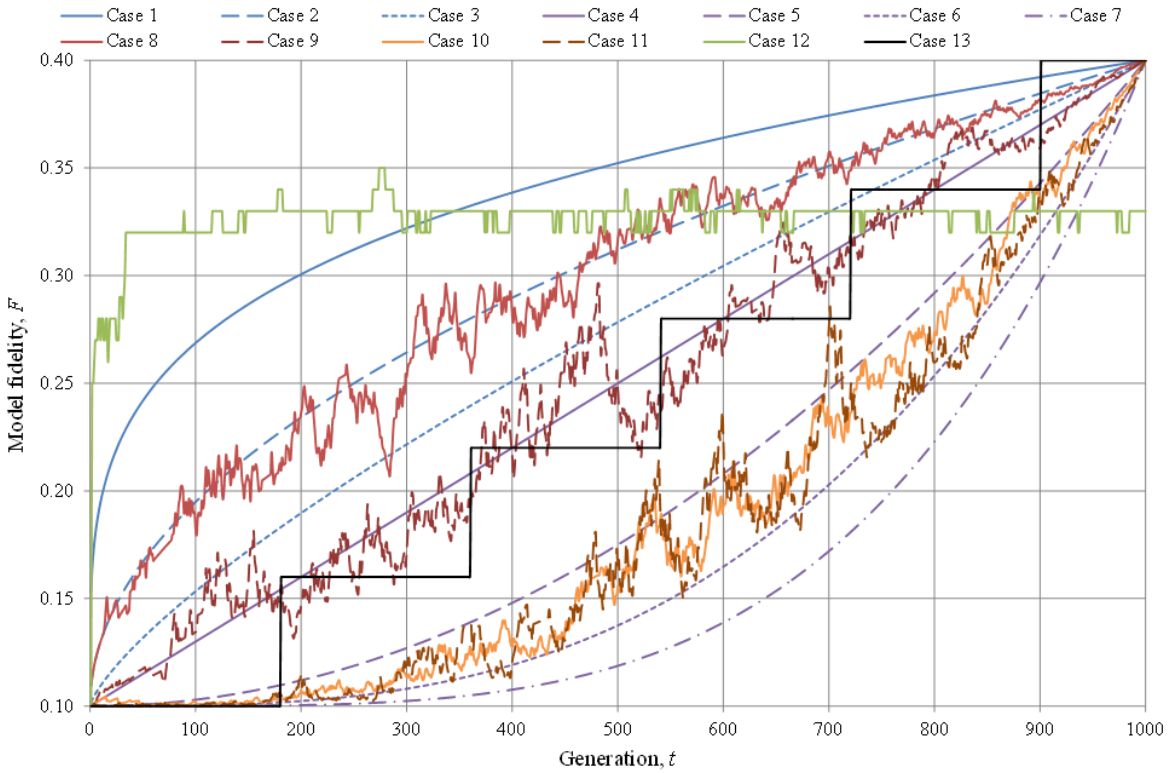

Figure 6. History of model fidelity during the optimisation generating results presented in Table 6.

The structural masses of the running optima during these experiments are shown in Figure 7. Early discovery of low-mass designs during Cases 1, 2 and 8 is evident during the first 100 generations. This resulted in early propagation throughout the population of designs with few structural members, leading to both reduced model size and computation time. Similarly, this occurred during Case 12 with self-adaptive control; however such gains in computation time were not possible due to each design of each population possessing an individual

fidelity level. The time taken to analyse in parallel each group of individual designs was dependent on the highest level of fidelity possessed by the individuals; therefore, the propagation of a high level of fidelity throughout the population from an early generation greatly increased the runtime. It is also evident in Figure 7 that major improvements in the designs occurred later in the process for Cases 5, 6, 7 and 10 than in other cases, i.e. from generation 725, due to the high values of δ and $\delta(t)$ lower bound discouraging high-fidelity modelling. Case 13 indicates an early generation of a good design, however failed to provide further significant improvements in the solution and generated the worst design of all cases in a longer time than Cases 1, 2, 3, 6 and 11.

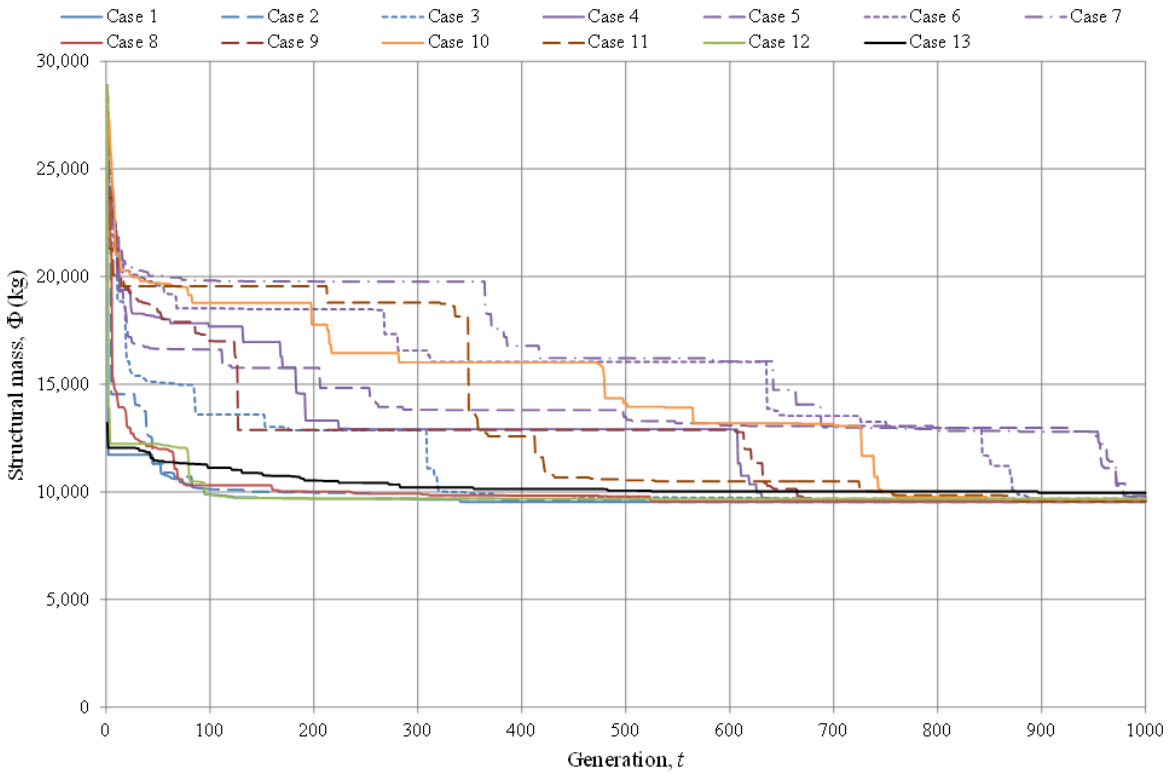

Figure 7. History of structural mass during the optimisation generating results presented in Table 6.

The best solutions generated during the study are subjected to further analysis to compare the feasibility of each design against the corresponding results obtained by FEA with F = 1.0. The differences in values measured with respect to the design constraints, $\Delta c_{1,2}$, are presented in Table 7 containing similar values to those listed in Table 2 during the investigation into the effects of fidelity on FEA. These results indicate that varying model fidelity during optimisation did not penalise the precision of feasibility measured during FEA compared to structural analysis at greatest fidelity.

Table 7. Variations in $\Delta c_{1,2}$ for best designs.

Case	F	Δc_1	Δc_2 (m)
1	0.33	0.2208	0.0003
2	0.33	0.2253	0.0002
3	0.33	0.1387	0.0018
4	0.33	0.1385	0.0002
5	0.40	0.0028	0.0005
6	0.33	0.2015	0.0001
7	0.38	0.0764	0.0002
8	0.32	0.2101	0.0002
9	0.33	0.1202	0.0060
10	0.32	0.1543	0.0002
11	0.33	0.1978	0.0003
12	0.33	0.0100	0.0000
13	0.34	0.2181	0.0086
F = 0.1	0.10	0.0000	0.0000
F = 0.2	0.20	0.6197	0.0006
F = 0.3	0.30	0.2478	0.0007
F = 0.4	0.40	0.0015	0.0001

The mean mass and computation time for each case is shown in Figure 8 alongside corresponding data for the experiments with varying levels of static model fidelity. Two thresholds are plotted in Figure 8 for the best

mean mass (F = 0.4) and computation time (F = 0.1) with static fidelity. The mean mass was lower during Cases 1, 2, 8, 11 and 12 than for F = 0.4; however no DCVFM case provided quicker computation than for F = 0.1. This was due to the gain in computation time associated with using low values of δ being reliant on early discovery of designs with few structural members. This did not always occur, in which case low values of δ led to more detailed analysis of large designs. Nevertheless, the mean times for all DCVFM cases were lower than that required using F = 0.4, i.e. the best design with static fidelity, except for Case 12 due to the independent level of fidelity possessed by population individuals resulting in lengthy structural analysis for each generation. These findings indicate that optimisation with DCVFM was capable of obtaining comparable, and sometimes better, solutions than the highest level of static fidelity whilst reducing the computation time required to do so. Notably, the approach representative of [14] during Case 13 generated a worse mean mass than all methods of DCVFM, with only static fidelity at F = 0.1 generating a solution of worse quality but over a significantly shorter period of time.

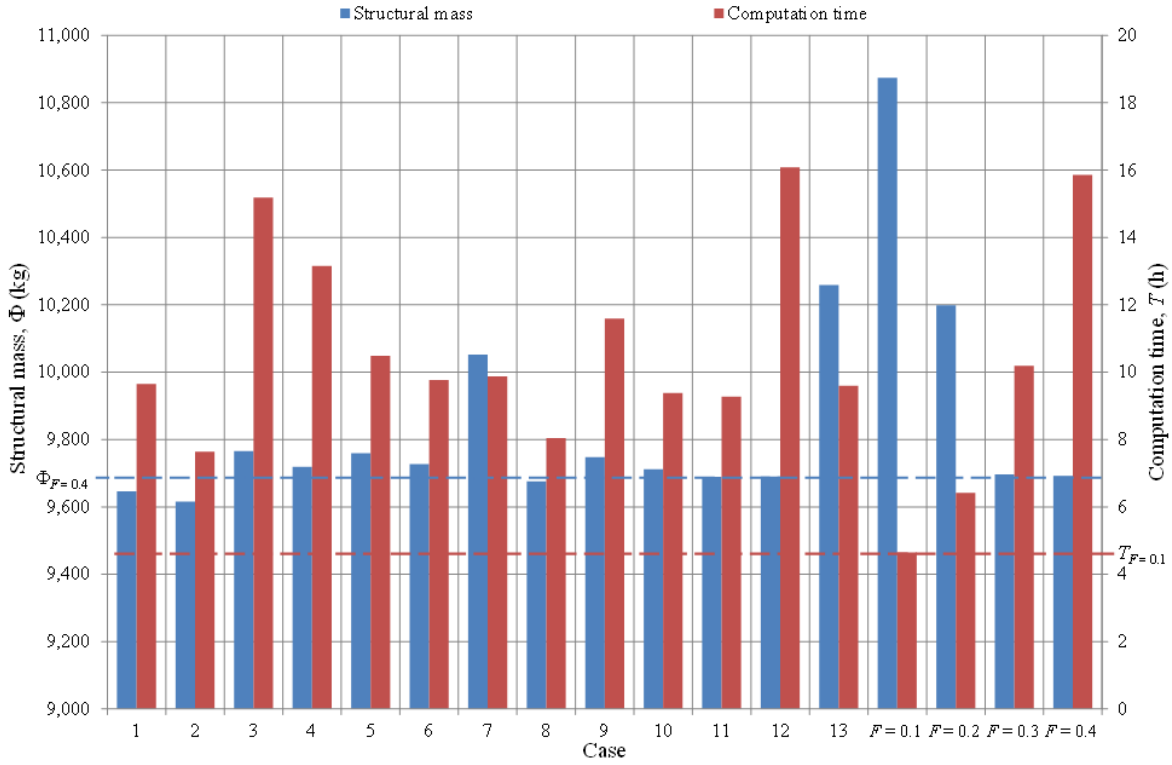

Figure 8. Mean structural mass and computation time during experimentation for different cases.

The results of this case study indicate that deterministic and hyper-heuristic parameter control generate the lightest aircraft designs at lowest computational cost. This was most noticeable with small values of δ or $\delta(t)$ to encourage early discovery of promising design traits before higher fidelity modelling to further improve a design. Self-adaptive control generated a mean solution of similar quality however at much higher computational cost due to the individual levels of model fidelity possessed by each population. Hence, coevolution of fidelity with the structural design failed to generate an improved parameter value over those defined by deterministic and hyper-heuristic parameter; thus indicating that solution quality was independent of model fidelity. Nevertheless, self-adaptive control did contain the best solution in all-but-one experiment

than all other cases during an early period of generations, e.g. as shown in Figure 7 for generation 95 to 340. This suggested future investigation of self-adaptive control, possibly interleaved with another parameter control method following this early period of good performance. The discrete method of parameter control representative of that employed in [14] produced the worst mean solution quality in a time greater than many cases using DCVFM.

The structural mass of the existing E-195 design may be estimated empirically using Table 1 as 11,954 kg [31]. Thus all designs in this study were lighter than the existing aircraft: the best herein weighing approximately 80% of the mass of the existing design (Case 1) and the worst about 91% (F = 0.1). However, this E-195 mass is an estimation based on the final aircraft design, which will have been designed to a greater level of detail than herein. Further, only a single load case was considered whereas the final design will have been analysed under numerous loads; which would be expected to increase the structural mass to maintain integrity. It is not possible to perform analysis of differences in the existing design and those herein due to a lack of public domain data regarding the airframe. Nevertheless, Figure 9 illustrates the evolution of the best airframe design obtained in this study to show the changes in number, position and distribution of structural members at specific generations during the optimisation process. This representation is of the airframe design, i.e. as in Figure 5, not the FE model at a specific fidelity level.

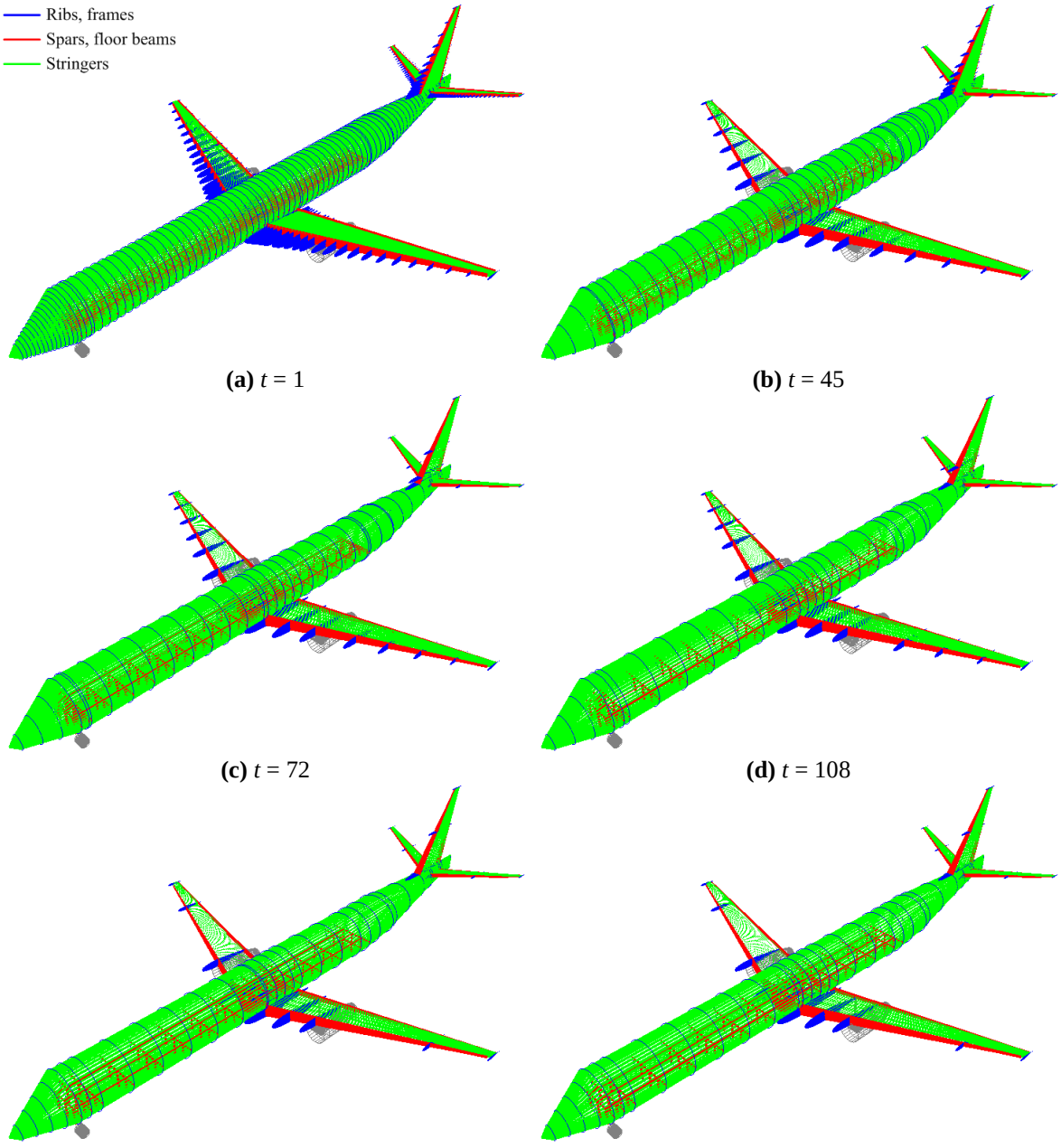

(a) t = 1 **(b)** t = 45

(c) t = 72 **(d)** t = 108

(e) t = 194 **(f)** t = 341

Figure 9. Evolution of overall best aircraft design generated during the study in Case 1.

5. Conclusion

A dynamic approach to variable-fidelity modelling has been presented for conceptual aircraft structural design optimisation such that computation time may be reduced whilst maintaining precision in structural analysis. This is accomplished through the encouraged use of low-fidelity models during early optimisation generations before increasing fidelity during later generations. DCVFM adapts fidelity using deterministic, hyper-heuristic or self-adaptive parameter control. The resulting FE model is constructed through the grouping of similar structural members for smeared model properties, followed by recovery of the stress field of members given obtained structural response through FEA.

The results of a case study indicated marginal difference in design feasibility when measured by FEA at different levels of model fidelity, with negligible difference at $F \geq 0.4$. Optimisation at a static high level of fidelity led to an improved design over that at low-fidelity but at an increase in computation time. Moreover, improvements were made in the qualities of aircraft designs generated and the required computation time when performing optimisation with DCVFM compared to using static fidelity modelling. This was most noticeable when utilising a low-fidelity model for a small number of generations at the start of optimisation before increasing fidelity, often leading to discovery of the final design earlier during the process than with static model fidelity. Further investigation of this behaviour is required such that the rules of DCVFM may be adapted to encourage such discovery and prevent excessive computation at high fidelity if further solution improvement is unlikely. Furthermore, optimisation with DCVFM produced considerably better solutions than a traditional approach to variable-fidelity modelling, in many cases in a reduced computation time.

The computational expense of aircraft structural design optimisation may be reduced whilst maintaining the quality of designs through dynamic control of model fidelity. Future investigations should include comparisons against other methods of reducing computation time, such as surrogate modelling, and further

experimentation using different methods and rules of parameter control, the interleaving of different parameter control methods and the consideration of various aircraft designs. The use of DCVFM for other aerospace design disciplines, e.g. aerodynamics, should be considered such that such computational benefits may be realised over a greater scope of the aerospace design domain, as well as optimisation subject to multiple load cases.

References

1. Antoine N, Kroo I, Willcox K and Barter G. A framework for aircraft conceptual design and environmental performance studies. In: *Proceedings of the 10th AIAA/ISSMO multidisciplinary analysis and optimization conference*, Albany, NY, USA, 30 August-1 September 2004, paper no. AIAA 2004-4314.
2. Kaufmann M, Zenkert D and Wennhage P. Integrated cost/weight optimization of aircraft structures. *Struct Multidiscip O*. 2010;41:325-334.
3. Allen JG, Coates G and Trevelyan J. A theoretical framework for the optimisation of the structural layout of an aircraft using deterministic and stochastic optimisation techniques. In: *Proceedings of the 8th ASMO-UK/ISSMO conference*, London, England, 8-9 July 2010, pp. 19-25.
4. Kesseler E and Vankan WJ. Multidisciplinary design analysis and multi-objective optimisation applied to aircraft wing. *Ele Com Eng*. 2006;1(2):221-227.
5. Schuhmacher G, Murra I, Wang L, Laxander A, O'Leary OJ and Herold M. Multidisciplinary design optimization of a regional aircraft wing box. In: *Proceedings of the 9th AIAA/ISSMO symposium on multidisciplinary analysis and optimization*, Atlanta, GA, USA, 4-6 September 2002, paper no. AIAA 2002-5406.
6. Amadori K, Jouannet C and Krus P. A framework for aerodynamic and structural optimization in conceptual design. In: *Proceedings of the 25th AIAA applied aerodynamics conference*, Miami, FL, USA, 25-28 June 2007, paper no. AIAA 2007-4061.

7. Hu TY and Yu XQ. Aerodynamic/stealthy/structural multidisciplinary design optimization of unmanned combat air vehicle. *Chinese J Aeronaut*. 2009;22:380-386.

8. Sobieszczanski-Sobieski J and Haftka RT. Multidisciplinary aerospace design optimization: survey of recent developments. *Struct Optimization*. 1997;14:1-23.

9. Böhnke D, Nagel B and Gollnick V. An approach to multi-fidelity in conceptual aircraft design in distributed design environments. In: *Proceedings of the IEEE aerospace conference*, Big Sky, MT, USA, 5-12 March 2011.

10. Neufeld D, Behdinan K and Chung J. Aircraft wing box optimization considering uncertainty in surrogate models. *Struct Multidiscip O*. 2010;42:745-753.

11. Barthelemy JFM and Haftka RT. Approximation concepts for optimum structural design – a review. *Struct Optimisation*. 1993;5:129-144.

12. Han ZH, Görtz S and Zimmermann R. Improving variable-fidelity surrogate modeling via gradient-enhancing kriging and a generalized hybrid bridge function. *Aerosp Sci Technol*. 2013;25(1):177-189.

13. Zheng J, Qui H and Feng H. The variable fidelity optimization for simulation-based design: a review. In: *Proceedings of the 2012 IEEE 16th international conference on computer supported cooperative work in design*, Wuhan, China, 23-25 May 2012, pp. 289-294.

14. Minisci E, Vasile E, Liqiang H. Robust multi-fidelity design of a micro re-entry unmanned space vehicle. *Proc IMechE Part G: Journal of Aerospace Engineering*. 2011;225:1195-1209.

15. Ricci S, Castellani M and Romanelli G. Multi-fidelity design of aeroelastic wing tip devices. *Proc IMechE Part G: Journal of Aerospace Engineering*. Epub ahead of print 18 September 2012. DOI: 10.1177/0954410012459603.

16. Allen JG, Coates G and Trevelyan J. Hyper-heuristic optimisation for application to aircraft structural design. In: *Proceedings of the 9th ASMO-UK/ISSMO conference*, Cork, Republic of Ireland, 5-6 July 2012, pp. 1-6.

17. Allen JG, Coates G and Trevelyan J. Approaches to parameter control for the optimisation of conceptual aircraft structural designs. In: *Proceedings of the 3rd RAeS aircraft structural design conference*, Delft, The Netherlands, 9-11 October 2012.

18. Howe D. *Aircraft loading and structural layout*. Bury St. Edmunds: Professional Engineering Publishing, 2004.

19. Niu MYC. *Airframe stress analysis and sizing*. 2nd ed. Conmilit Press: Hong Kong, 1999.

20. Roark RJ and Young WC. *Formulas for stress and strain*. 5th ed. New York: McGraw-Hill, 1975.

21. Cowling P, Kendall G and Soubeiga E. A hyperheuristic approach to scheduling a sales summit. *Lect Notes Comput Sc*. 2000:176-190.

22. Burke EK, Hyde M, Kendall G, Ochoa G, Ozcan E and Qu R. *Hyper-heuristics: a survey of the state of the art*. University of Nottingham. Report no. NOTTCS-TR-SUB-0906241418-2747, 2010.

23. Kirkpatrick S, Gelatt CD and Vecchi MP. Optimization by simulated annealing. *Science*, 1983;220(4598):671–680.

24. Meyer-Neiberg S and Beyer HG. Self-adaption in evolutionary algorithms. In: Lobo FG, Lima CF and Michalewicz Z (eds) *Parameter setting in evolutionary algorithms*. Berlin: Springer-Verlag, 2007, pp. 47-76.

25. Embraer SA. Embraer 195 airport planning manual, October 2011.

26. Jackson P. *Jane's all the world's aircraft 2009-2010*. Coulsdon: Jane's Information Group, 2009, pp. 43-46.

27. Trimble S. Embraer commits to re-engined E-jets. *Flightglobal*, http://www.flightglobal.com/news/articles/embraer-commits-to-re-engined-e-jets-364603 (2011, accessed 10 December 2012).

28. CS-25:2012. Certification specifications and acceptable means of compliance for large aeroplanes.

29. Youn B, Choi KK, Yang R and Gu L. Reliability-based design optimization for crashworthiness of vehicle side impact. *Struct Multidiscip O*. 2004;26:272-283.

30. Sensmeier MD and Samareh JA. A study of vehicle structural layouts in post-WWII aircraft. In: *Proceedings of the 45th AIAA/ASME/ASCE/AHS/ASC structures, structural dynamics and materials conference*, Palm Springs, CA, USA, 19-22 April 2004, paper no. AIAA 2004-1624.

31. Torenbeek E. *Synthesis of subsonic airplane design*. Dordrecht: Kluwer Academic Publishers, 1982, p. 266.

Appendix 1

Notation

A^e cross-sectional area of *e*th element (m^2)

A^i cross-sectional area of ith element member (m^2)

b lifting surface span (m)

c_w wing chord length (m)

c_1 design constraint for minimum FoS under yield as defined by von Mises criterion

c_2 design constraint for maximum wingtip deflection (m)

C rib distribution constant

E^e elastic modulus of eth element (Pa)

E^i elastic modulus of ith element member (Pa)

$\boldsymbol{f}$ excitation vector

f_j^e internal force in eth element in jth DoF (N)

f_j^i internal force in ith element member in jth DoF (N)

F model fidelity level

$F(t)$ model fidelity level at generation t

$F_{\max}$ maximum constraint on model fidelity level

$F_{\min}$ maximum constraint on model fidelity level

G^i shear modulus of ith element member (Pa)

i counter of element member number

$I_p{}^i$ polar second moment of area about x-axis of ith element member (m^4)

$I_{yy}{}^i$ cross-sectional second moment of area about y-axis of ith element member (m^4)

$I_{zz}{}^i$ cross-sectional second moment of area about z-axis of ith element member (m^4)

j counter of DoF number

k counter of element member number

$\mathbf{K}$ stiffness matrix

l^i length of ith element member (m)

n_{DoF} number of DoF

n_m number of element members

n_r number of ribs

r rib number

t generation number

$t_{\max}$ total number of generations

T total computation time (h, s)

$T(t)$ computation time for generation t (h)

$\boldsymbol{u}$ response vector

u_x^e axial extension of eth element (m)

$v_{1,\ldots,16}$ design variables

y_0 position of root rib in spanwise direction (m)

y_r position of rth rib in spanwise direction (m)

α rib distribution factor

$\beta(t)$ generation number weighting factor

γ_j^i internal force distribution factor of ith element member in jth DoF

γ_j^k internal force distribution factor of kth element member in jth DoF

δ model fidelity rate of change

$\delta(t)$ model fidelity rate of change at generation t

Δc_1 difference in values of design constraint for minimum FoS by von Mises criterion

Δc_2 difference in values of design constraint for maximum wingtip deflection (m)

ΔF change in model fidelity level

$\phi(t)$ hyper-heuristic objective at generation t

$\phi_1(t)$ design objective component of hyper-heuristic objective at generation t

$\phi_2(t)$ computation time component of hyper-heuristic objective at generation t

$\Phi(t)$ design objective at generation t